Pressure-modulated competition between dual charge density waves in $NbSe_3$

Yongsheng Zhao,[1,2] Konstantin Glazyrin,[2] Pablo J. Bereciartua,[2] Christian Plueckthun,[2] Satishkumar Kulkarni,[3] Nana Li,[1] Limin Yan,[1,4] Kai Zhang,[1] Bihan Wang,[1,2] Yiming Wang,[1] Jianbo Zhang,[1] Nico Giordano,[2] Helmuth Berger,[5] Xin Wang,[6] Sonia Francoual,[2,*] Wenge Yang,[1,†] and Moritz Hoesch[2,‡]

[1]*Center for High Pressure Science and Technology Advanced Research (HPSTAR), 1690 Cailun Road, Shanghai 201203, People's Republic of China*

[2]*Deutsches Elektronen-Synchrotron DESY, Notkestrasse 85, 22607 Hamburg, Germany*

[3]*Centre for X-ray and Nano Science CXNS, Deutsches Elektronen-Synchrotron DESY, Notkestrasse 85, 22607 Hamburg, Germany*

[4]*School of Science, Inner Mongolia University of Science and Technology, Baotou 014010, People's Republic of China*

[5]*École Polytechnique Fédérale de Lausanne (EPFL), 1015 Lausanne, Switzerland*

[6]*State Key Laboratory of Superhard Materials, Department of Physics, Jilin University, Changchun 130012, People's Republic of China*

(Received 10 November 2025; revised 2 February 2026; accepted 9 April 2026; published 18 May 2026)

Controlling collective electronic states through clean and reversible external stimuli is crucial for realizing functional quantum materials. Here, we report a study on temperature (T) and pressure (P)-tuned charge-density-wave (CDW) orders in the quasi-one-dimensional system of $NbSe_3$, through single-crystal x-ray diffraction, and electric and magnetotransport measurements. A refined and extended phase diagram is presented, prompting a reevaluation of earlier claims regarding the coexistence of CDW and superconductivity (SC). Here, SC is found to emerge only once all long-range CDWs are suppressed. Notably, the anomalous Hall and magnetoresistance (MR) effects observed at low pressure (LP ~ 0.8 GPa) may arise from distinct carrier types associated with the two competing CDWs, CDW1 and CDW2. These two coexisting CDWs, characterized by distinct modulation vectors, $\boldsymbol{q_1}$ and $\boldsymbol{q_2}$, show pressure-induced opposing shifts in their b^* axis projections (denoted as q_1^{b*} and q_2^{b*}), while preserving a phase-coupling relationship $2(\boldsymbol{q_1}+\boldsymbol{q_2}) \sim [111]$. Upon gradual suppression of the long range order CDW2 order, q_1^{b*} of CDW1 stabilizes and enters a decoupled regime within $\sim$0.8−1.3 GPa, followed by a pronounced change in its periodicity between $\sim$1.3 and 2.9 GPa. Above 2.9 GPa, all long-range CDW orders vanish, giving way to emergent superconductivity (SC).

DOI: 10.1103/s48z-19pt

I. INTRODUCTION

Quasi-one-dimensional (q1D) systems [1,2] exhibit distinctive magnetotransport behavior compared to two- or three-dimensional (2D or 3D) counterparts, largely due to their tendency to stabilize charge-density-wave (CDW), or spin-density-wave (SDW) states. Superconductivity (SC), when observed in a truly one-dimensional electronic band, is necessarily nonconventional in character. Despite intensive study over half a century, a comprehensive understanding and generalization of these systems remain elusive. Strong electronic correlations give rise to complex phenomena that are still underexplored.

$NbSe_3$ stands out as an archetypical linear-chain compound, notable for hosting two distinct CDWs [3,4]. It serves as a model system for exploring unconventional physics of the pseudo-1D metals. The two incommensurate CDWs emerge with modulation wave vectors $\boldsymbol{q_1}$ =(0, 0.241, 0) at $T_{\mathrm{CDW1}} = 145$ K and $\boldsymbol{q_2}$ =(0.5, 0.259, 0.5) at $T_{\mathrm{CDW2}} = 59$ K [1,5–7]. Both vectors are remarkably noncollinear [8] and display complex spatial distributions [9,10]. First-order, second-order, and third-order CDW satellite peaks have been observed in Fourier transform of scanning tunneling microscopy (STM) images [9]. Furthermore, additional weaker satellite peaks have been reported (type $\mathbf{m}\cdot\boldsymbol{c}^* + \mathrm{n}\cdot\boldsymbol{q_1} + \mathrm{p}\cdot\boldsymbol{q_2}$), suggesting that some electronic states are simultaneously modulated by both CDWs [9,11].

Adding further complexity, recent angle-resolved photoemission spectroscopy (ARPES) studies suggest that the two CDW orders in $NbSe_3$ at low temperature arise from self-organization inside orbitally distinct electronic systems [12], along with higher-dimensional interactions that help stabilize the CDW states in this quasi-1D (q1D) material [13]. These q1D systems are known to be highly sensitive to external stimuli, such as electric field [14–19], strain [20–22], and pressure (P) [23–28]. In $NbSe_3$, the electronic field-induced CDWs periodicity change ($\boldsymbol{q}$ wave-vector shift) [15,18,29], suggests the possibility of joint commensurability between the two CDWs: a phase-coupling relationship $2(\boldsymbol{q_1}+\boldsymbol{q_2}) \sim [111]$ [16,30]. Such variations of the CDW periodicity [15,18,29]

*Contact author: sonia.francoual@desy.de
†Contact author: yangwg@hpstar.ac.cn
‡Contact author: moritz.hoesch@desy.de

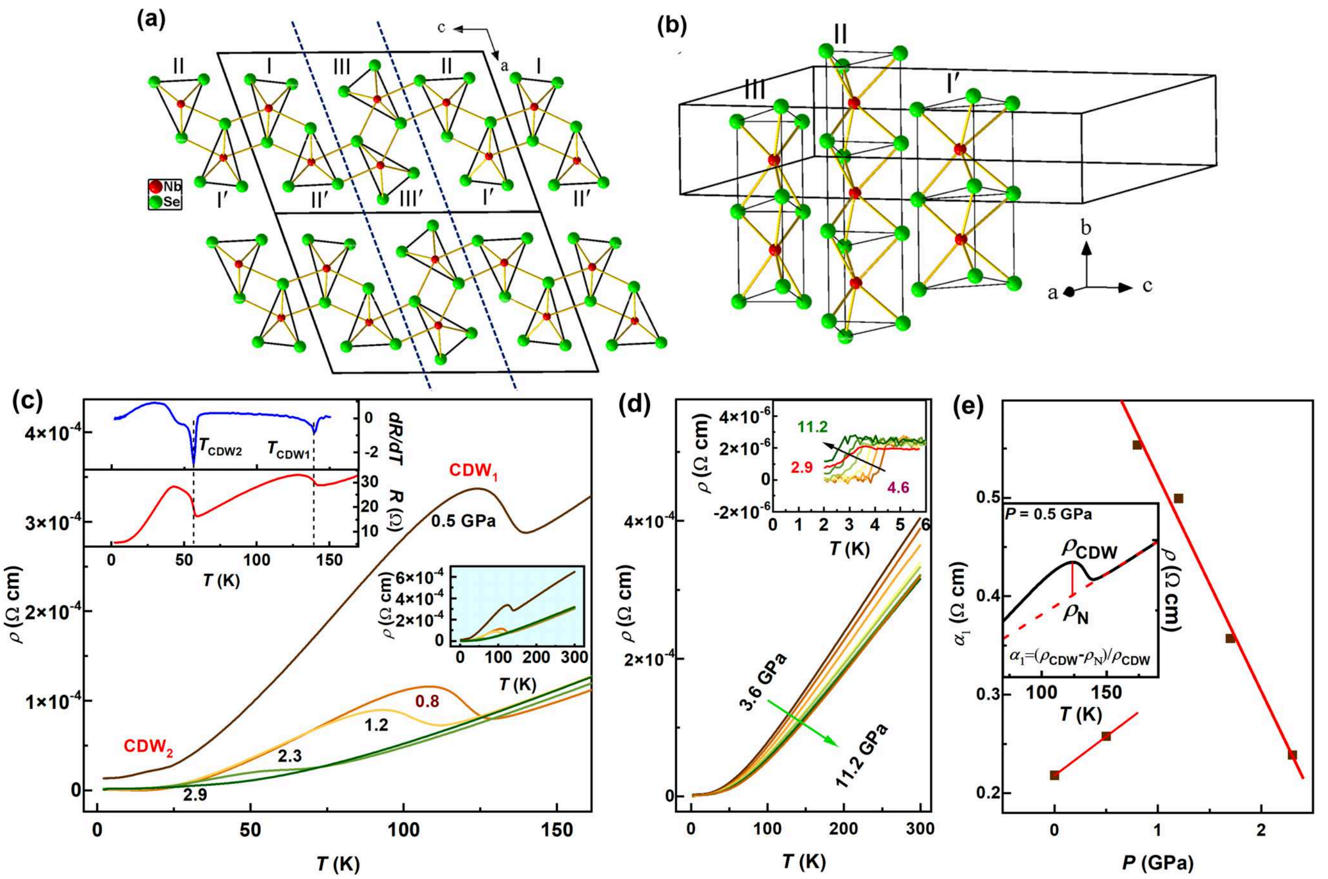

FIG. 1. (a) Unit cell of $NbSe_3$ with the three pairs of inequivalent triangular prism chains. The pair of chains III and III' forms a "double unit" while the two pairs of chains, II and II', and I and I', form a "quadruple" unit. Quadruple and double units are separated by a blue-black dashed line. Two pairs of chains III and III' (I and I') form the dipole CDW. Details are given in the text. (b) View of the three inequivalent chains running along the *b* axis. Individual atoms forming the unit cell, as well as their atomic coordinate *y*, are indicated. (c) Resistivity $\rho(T)$ measurements of $NbSe_3$ between ~0.5 and 2.9 GPa for $T \sim 2-160$ K; the left inset shows the ambient pressure resistance $R(T)$ (in red) and its derivative dR/dT (in blue); the right inset shows the full resistivity $\rho(T)$ curve for $T \sim 2-300$ K. The current ($I = 500\,\mu$A) was applied along the *b* axis. (d) $\rho(T)$ between ~2.9 and 11.2 GPa. Inset: magnified view of the low-*T* range ($T < 5$ K). The pumpkin patch colors are stretching with increasing *P*. (e) The *P* dependence of α_1 parameter. The inset shows the definition of ρ_{CDW}, ρ_N, and α_1 in the case of CDW1 formation at $P = 0.5$ GPa.

are often observed alongside CDW sliding phenomena, as extensively reported in Refs. [14–19]. Numerous transport studies [25,31–35] on $NbSe_3$, under elevated pressures, have shown that both CDWs are progressively suppressed with increasing pressure, but at distinct critical pressure values. Previous reports also suggest the emergence of two separate SC phases, with one phase potentially coexisting with CDW1 [31]. While x-ray diffraction offers direct insight into the spatial distribution and evolution of CDWs under pressure, to the best of our knowledge, no high-*P* single-crystal x-ray diffraction measurements of $NbSe_3$ have been previously reported.

In this work, we revisit the low *T* and high *P* phase diagram of $NbSe_3$ using high-resolution single-crystal x-ray diffraction, complemented by transport measurements performed on the same single-crystal specimen. This combined approach allows for a more comprehensive understanding of the (*T*, *P*) phase diagram, particularly regarding the suppression of long-range CDW1 and CDW2, and the appearance of the SC dome. Among our key findings, we report a *P*-induced change in CDW periodicity and provide evidence of phase coupling between CDW1 and CDW2 in their coexistence regime. These effects are reflected in the evolution of their reciprocal space features, which we discuss in detail below.

$NbSe_3$ crystallizes into a monoclinic structure with space group $P2_1/m$ (No.11). The unit cell of $NbSe_3$ contains three pairs of inequivalent metallic chains, as shown in Fig. 1(a): type I, II, and III, formed by $NbSe_3$ triangular prisms stacked in the *ac* plane. CDW1 associated with wave vector $\boldsymbol{q_1}$ primarily resides on Nb atoms in type III chains and CDW2 related with $\boldsymbol{q_2}$ mainly on type I chains [13]. These chains run along the monoclinic *b* direction, with type I and III chains featuring very short Se-Se triangular sides (isosceleslike), while the type II chains are much longer (closer to equilateral).

Following the convention in Ref. [36], each $NbSe_3$ layer can be divided into a six-chain system comprising a four-chain "quadruple" unit (two type I chains flanked by two type II chains, denoted I' and II') and a two-chain "double" unit (a pair of type III chains, denoted III'). These structural blocks are illustrated in Fig. 1(a), separated by a dark blue dashed line. Along the *b* direction, two adjacent chains are displaced by half a unit cell vector, with Nb atomic positions located at fractional *y* coordinate of 1/4 and 3/4 as indicated in Fig. 1(b). Each Nb atom is coordinated with six Se atoms from its own chain and two additional Se atoms from the neighboring chains, forming eight-coordinate $NbSe_3$ layers in the *bc* plane. Importantly, both type I/I' and type III/III' form dipolelike CDWs through interchain coupling, resulting in paired-chain configuration [13,37]. This dipole nature of CDWs may influence charge transport by modulating the electron density distribution, potentially reducing sensitivity to point defects such as cation vacancies [5,38].

Single-crystal diffraction data at ambient pressure and room temperature are shown in Fig. S1 of Supplemental Material [39], while structural refinements at ambient P ($T = 293$ K) and high P ($T = 32$ K) are presented in Tables S1 and S2 of Supplemental Material [39]. These crystallographic results are consistent with prior studies [6,36–38], and additional experimental details are provided in Supplemental Material [39]. It is important to note that, at low temperature, the presence of one or even two additional incommensurate modulation wavevectors ($\boldsymbol{q_1}$ and $\boldsymbol{q_2}$) to properly index the diffraction pattern is a characteristic feature of an aperiodic crystal. A comprehensive description of these types of structures requires the superspace formalism, which is complex and outside the scope of this study. Therefore, the structural analyses performed in this work have been restrained to the set of reflections that can be indexed rationally using the three reciprocal vectors a^*, b^*, and c^*. An exhaustive and accurate structural determination of these two incommensurately modulated phases could be addressed in an additional study. The corresponding findings, as determined from our data structural and transport measurements, are presented in the "Results" and "Discussion" sections below.

II. RESULTS

The crystalline quality of the $NbSe_3$ samples was assessed through the sharpness of the CDW-related resistive anomalies and the residual resistivity ratio ($\mathrm{RRR} = R_{300\,\mathrm{K}}/R_{4.2\,\mathrm{K}}$). Our ambient pressure transport measurements are shown in the inset of Fig. 1(c). Two clear and well-defined anomalies associated with the CDW transitions are observed at $T_{\mathrm{CDW1}} = 145$ K and $T_{\mathrm{CDW2}} = 59$ K [8,34], with a residual resistivity ratio (RRR) of ~16, comparable to previous reports [40–42]. The T dependence of resistivity R(T), along with its derivative dR/dT [insert of Fig. 1(c)], reveals two distinct anomalies corresponding to the onset of the CDW transitions. As expected, applying external pressure alters the electronic structure and phase stability of $NbSe_3$. This is reflected in the P-dependent resistivity behavior, as illustrated in Figs. 1(c) and 1(d), where clear P-induced modification in $\rho(T)$ are observed.

The data presented in Fig. 1(c) capture the evolution of the resistivity under pressure up to ~2.9 GPa over the temperature range of 2–160 K, while Fig. 1(d) extends this view to higher pressures, reaching ~11.2 GPa, and spans the full temperature range of 2–300 K. At 0.5 GPa, the residual resistivity ratio RRR is approximately 47. This value is comparable in magnitude to the RRR values typically reported for $NbSe_3$ single crystals at ambient pressure prior to high-pressure experiments (~50–60) [31,32].

The resistive increments at T_{CDW1} and T_{CDW2} result from the opening of a gap at the Fermi level E_{F} due to the CDW formation. The size of the resistive increment is usually defined as

$$\alpha = (\rho_{\mathrm{CDW}} - \rho_{\mathrm{N}})/\rho_{\mathrm{CDW}} = \Delta N/N_0.$$

Here, ρ_{CDW} is the resistivity in the CDW state, and ρ_{N} is the resistivity that would be expected in the absence of the CDW formation [31,33]. N_0 represents the density of state at E_{F} in the normal (non-CDW) state, and ΔN denotes reduction of N_0 due to the CDW1 formation. The parameter α thus provides information about the size of the nesting area at the Fermi surface. As shown in Fig. 1(e) for CDW1, α_1 shows a sharp increase at ~0.8 GPa and then gradually decreases up to ~2.3 GPa. The inset of Fig. 1(e) schematically illustrates how ρ_{CDW} and ρ_{N} are defined. The ρ_{N} is estimated by linearly extrapolating the resistivity from above T_{CDW1} down to lower T. However, as the CDW2 is extremely sensitive to P, α_2 is hard to be determined with P.

With increasing pressure, T_{CDW1} exhibits a gradual suppression to ~2.9 GPa, while T_{CDW2} is rapidly quenched and becomes undetectable above ~0.5 GPa. The inset of Fig. 1(d), highlights the low-temperature region, where a distinct drop in ρ(T) indicates the formation of a superconducting state in $NbSe_3$. The onset temperature of the superconductivity, T_{c}, is highly pressure dependent and a zero-resistance state is realized at $P = 4.6$ GPa. The maximum T_{c} in our study reaches ~4.5 K at this pressure. We identify a SC dome spanning the pressure range from ~2.9 to 11.2 GPa. The corresponding (T, P) phase diagram is summarized in Fig. 2.

The magnetic field dependence of the Hall resistance $R_{\mathrm{xy}}(B)$ and magnetoresistance (MR), derived from the longitudinal resistance $R_{\mathrm{xx}}(B)$, at selected temperatures and pressures, are presented in Figs. 3(a)–3(d) and Figs. 3(e) and 3(f), respectively. The experimental geometry for current and magnetic field orientation is carefully considered and detailed in Supplemental Material [39]. The sign of the derivative of $R_{\mathrm{xy}}(B)$ (slope) is used to identify the dominant carrier type, where a positive slope corresponds to holelike (*p*-type) carriers and a negative slope to electronlike (*n*-type) carriers.

At a representative pressure of ~0.5 GPa [Figs. 3(a) and 3(b)], a nonlinear behavior in $R_{\mathrm{xy}}(B)$ emerges at around $B \sim 4$ T at both $T = 2$ and 10 K, indicative of a competition between *n*-type and *p*-type carriers. This behavior is consistent with prior observations at ambient pressure [43,44], where multiband or mixed-carrier effects produce similar crossover features. As the pressure increases beyond ~0.8 GPa, $R_{\mathrm{xy}}(B)$ becomes entirely negative over the full magnetic field range [Figs. 3(c) and 3(d)], indicating the dominance of *n*-type carriers up to the maximum pressure investigated (7.9 GPa).

In the low-field regime, $B < 2$ T, $R_{\mathrm{xy}}(B)$ displays a linear dependence on B, enabling the extraction of the Hall coefficient per unit thickness, R_{H}/d, via

$$R_{\mathrm{H}} = d \times R_{\mathrm{xy}}(B)/B = 1/N_{\mathrm{e}}e,$$

where d is the sample thickness and N_{e} is the carrier density. The evolution of R_{H}/d with P is shown in Fig. 3(g), revealing a pronounced minimum between ~0.8 and 1.2 GPa,

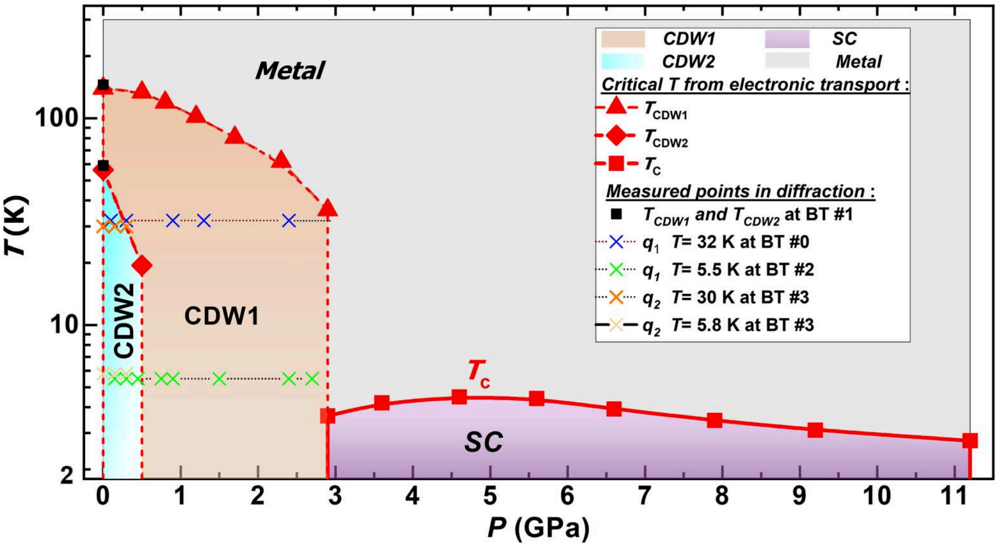

FIG. 2. Phase diagram of $NbSe_3$ determined from our study. The CDW $\boldsymbol{q}_1$ vector persists up to $\sim$2.9 GPa, while $\boldsymbol{q}_2$ is suppressed at $\sim$0.5 GPa, as revealed by our diffraction measurements. The phase boundary, derived from transport measurements, aligns with our diffraction results.

corresponding to a local maximum in N_e, which signals a reconstruction of the Fermi surface. This pressure range coincides with the suppression of the long-range CDW2 states, suggesting a strong coupling between the CDW2 order and the electronic structure near the Fermi level. While this minimum becomes less prominent at elevated temperature due to thermal broadening or suppression of the long-range CDW2 order, it remains clearly discernible even at 120 K.

The MR data sets [Figs. 3(e) and 3(f)] show further evidence for this carrier-type crossover. A positive MR is observed at $P = 0.5$ GPa ($T = 2$, 10, and 120 K), typically associated with p-type or multiband transport. At

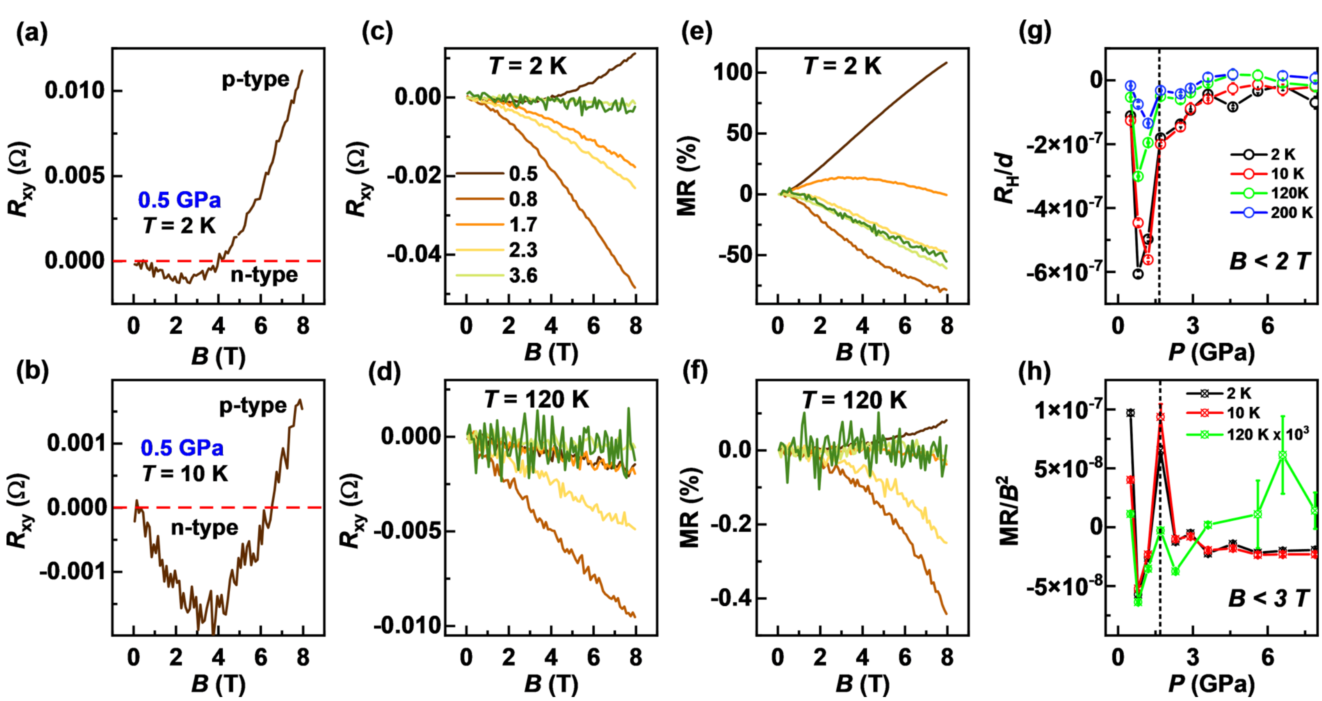

FIG. 3. (a)–(d) Hall resistance (R_{xy}) as a function of the magnetic field up to 9 T recorded at different pressures and temperatures: (a) 2 K and 0.5 GPa; (b) 10 K and 0.5 GPa; (c) 2 K and $\sim$0.5–7.9 GPa; (d) 120 K and $\sim$0.5–7.9 GPa. (e),(f) Longitudinal magnetoresistance (MR) as a function of the magnetic field in the range 0–9 T (e) $T = 2$ K and $\sim$0.5–7.9 GPa; (f) 120 K and $\sim$0.5–7.9 GPa. (g) R_H/d ($B < 2$ T; see text) as a function of P at different T. Error bars are shown, if not visible, they are smaller than or equal to the symbols size. In (h), we show the fitting parameters of MR/B^2, obtained by applying a quadratic polynomial model to the MR data in the low magnetic field range at different T. Error bars are also indicated.

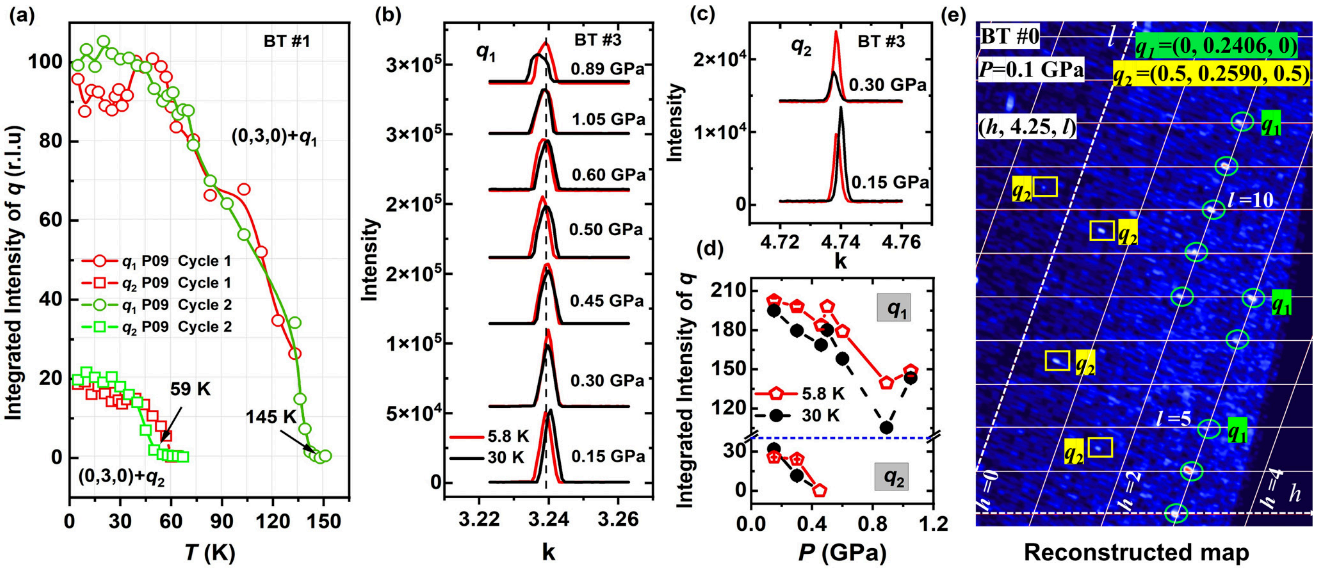

FIG. 4. (a) T-dependent intensity of satellite reflections $\boldsymbol{q_1}$ and $\boldsymbol{q_2}$ at ambient pressure for the first beamtime (BT #1) for low T and ambient pressure collected at the P09, PETRA III using a point detector. Data were collected for two cycles corresponding to warming up from low $T = 5$ K to the highest $T = 151$ K. The black arrows indicate the suppression of the long-range CDW1 ($T_{\mathrm{CDW1}} = 145$ K) and CDW2 ($T_{\mathrm{CDW2}} = 59$ K) order associated with $\boldsymbol{q_1}$ and $\boldsymbol{q_2}$ vectors, respectively. (b) k scan (BT #3) through the satellite reflection $(0, 3, 0) + \boldsymbol{q_1}$ at $T = 5.8$ K (red) and $T = 30$ K (black) with selected pressure to highest ~1.05 GPa. For the sake of completeness, we note that the data collection at ~0.89 GPa followed the data collection at ~1.05 GPa. (c) k-scan third beamtime (BT #3) through the satellite reflection $(0, 5, 0) + \boldsymbol{q_2}$ at $T = 5.8$ K and $T = 30$ K with $P = 0.15$ and 0.3 GPa, respectively. (d) Integrated intensity of satellite reflections (BT #3) at $\boldsymbol{q_1}$ and $\boldsymbol{q_2}$ at $T = 5.8$ and 30 K as a function of pressure. (e) Integration along b^* of a region of the reconstructed reciprocal space with Miller indices $(h, 4.25, l)$ (P02.2, BT #0, $P = 0.1$ GPa). The integration covers a range in k from 4.23 to 4.27 to visualize simultaneously the two sets of reflections present when CDW1 and CDW2 coexist. The reflections associated with modulation wave vectors $\boldsymbol{q_1}$ and $\boldsymbol{q_2}$ are highlighted inside green circles and yellow rectangles, respectively.

$P \sim 0.8$ GPa, the MR becomes consistently negative, suggesting an enhanced scattering or mobility suppression. Notably, a reappearance of positive MR is detected around ~1.7 GPa at $T = 2$ and 10 K, indicating a nonmonotonic pressure evolution of the band structure or carrier dynamic.

These results are consistent with previous reports [17], which describe a quadratic B^2 dependence of MR under n-type conduction (negative Hall voltage) at low magnetic fields, and a linear B behavior under p-type conduction (positive Hall voltage) at higher fields. To quantify the field dependence, we fitted the low-field MR data using the form:

$$\mathrm{MR} = \kappa \times B^2,$$

at $T = 2$, 10, and 120 K. The extracted fitting parameters, MR/B^2, are presented in Fig. 3(h). While the observed extrema at ~0.5 , 0.8, and 1.7 GPa do not correspond to any clear phase boundaries in the phase diagram of Fig. 2, they seem to match with the inflection points in R_{H}/d in Fig. 3(g). This correlation strongly supports the interpretation that the observed MR behavior originates from a carrier-type crossover and an associated reorganization of the electronic band structure.

Multiple crystals from the same growth batch as those used for the electrical transport measurements were screened for the single-crystal x-ray diffraction experiments, finding that many of them were twinned (see Supplemental Material [39] for details). We note that twinning in $NbSe_3$ has been previously observed and reported [3]. Suitable crystals for performing diffraction studies at both ambient and high pressure were selected. The high-pressure x-ray diffraction results are presented in Figs. 4 and 5. Our single-crystal data confirm the stability of the monoclinic phase throughout the full pressure range of our study (see Table S2 and Fig. S2 in Supplemental Material [39] for additional details). This provides an indication that the P-induced evolution of the long-range CDW wave vectors, $\boldsymbol{q_1}$ and $\boldsymbol{q_2}$, likely reflects changes mainly affecting the electronic structure [26], which we briefly discuss below.

At ambient pressure, reflections associated with the $\boldsymbol{q_1}$ and $\boldsymbol{q_2}$ wave vectors disappear above their respective transition temperatures, $T_{\mathrm{CDW1}} = 145$ K and $T_{\mathrm{CDW2}} = 59$ K, as shown in Fig. 4(a). This disappearance aligns with the phase boundary derived from the transport measurements (see Fig. 2).

CDW1 reflections remain detectable up to ~2.7 GPa, as confirmed in two independent beamtimes (BT #0 and #2). The integrated intensities of reflections associated with $\boldsymbol{q_1}$ and $\boldsymbol{q_2}$, plotted in Fig. 4(d), reveal the suppression of the long-range CDW2 order near ~0.45 GPa. Notably, the intensities of CDW2 satellites are roughly five times weaker than those of CDW1, potentially explaining their reduced visibility at higher incident beam energies and in data obtained in the area-detector run (BT #0). Nevertheless, several $\boldsymbol{q_2}$ reflections were observed at $P = 0.1$ and 0.3 GPa in the reconstructed reciprocal space layers, as shown in Fig. 4(e) (BT #0, $P = 0.1$ GPa). This intensity map was obtained by integrating a region of the reconstructed reciprocal space (along b^*) over a narrow k window (from $k = 4.23$ to 4.27) centered at $k = 4.25$. This figure allows the simultaneous visualization of reflections

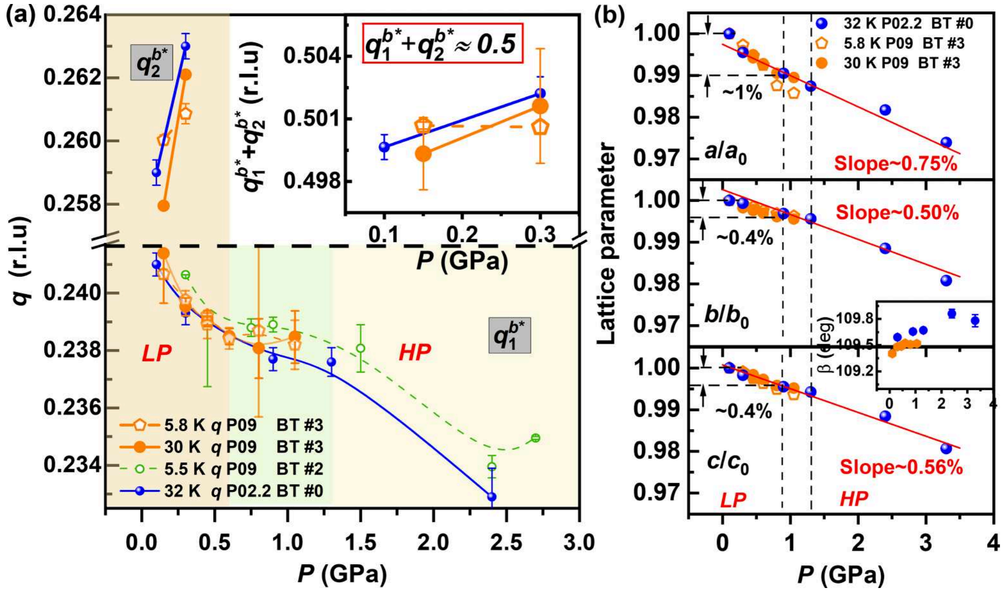

FIG. 5. (a) P-dependent reciprocal lattice components q_1^{b*} and q_2^{b*} of the long-range CDW modulation vector $\boldsymbol{q_1}$ and $\boldsymbol{q_2}$ measured for BT #2–3 and BT #0 of PETRA III. The inset shows the sum of $q_1^{b*} + q_2^{b*}$ in relation to the value of 0.5 as a function of P. Here and below, we indicate data collected at BT #0 and BT #2–3 using blue and green/orange symbols, respectively. (b) P-dependent refined and normalized lattice parameters. The red lines represent linear fits as visual guides, with the extracted slopes indicated. The low-pressure range (LP, $0 < P < 0.8$ GPa) and the high-pressure range (HP, $1.3 \leqslant P \leqslant 3.3$ GPa) are labeled accordingly. The inset compares the data on the monoclinic β angle measured at BT #0 and BT #2.

associated with the modulation vectors $\boldsymbol{q_1}$ and $\boldsymbol{q_2}$, and excludes any main Bragg reflection at $k = 4$ or 5. At ~0.8 GPa, the $\boldsymbol{q_2}$ modulation features have completely vanished as observed in BT #3 and BT #0.

The P dependence of the long-range CDW wave vectors $\boldsymbol{q}$ projected along the b direction is summarized in Fig. 5(a). Throughout this work, we refer to the $b*$ axis projection of these vectors as q_1^{b*} and q_2^{b*}, respectively. Both q_1^{b*} and q_2^{b*} exhibit clear shifts with increasing P, indicating a pressure-induced change in the periodicity of the CDW modulations. The shifts of these two low-temperature CDW wave vectors have opposite signs in the b^* component. We note that at the lowest P values, $q_1^{b*} = 0.241$ and $q_2^{b*} = 0.259$ slightly differ from the ambient pressure values of $q_1^{b*} = 0.24$ and $q_2^{b*} = 0.26$ at $T = 30$ K (Ref. [14]). But the overall trends are consistent. An increase in q_2^{b*} is observed in the narrow range prior to the complete disappears of the long-range CDW2 at ~0.5 GPa. q_1^{b*} decreases with P until ~0.8 GPa, then plateaus (or inflects) before decreasing again from ~1.3 GPa to ~2.9 GPa, with complete suppression of the long-range CDW1 order signal at higher pressure. Unlike q_1^{b*}, the value of q_2^{b*} increases with P. Interestingly, the sum of $q_1^{b*} + q_2^{b*}$ remains approximately constant at ~0.5 over the entire pressure range, as shown in the inset of Fig. 5(a). This observation, within error margins, likely reflects a persistent phase-coupling relationship between the two CDWs within their coexistence regime [16,30].

The position of $\boldsymbol{q_1}$ (associated with CDW1 distortion) exhibits complex and P-sensitive behavior. In contrast, the main crystal lattice displays no significant anomalies, especially for the lattice parameters as seen in Fig. 5(b). We only note that below ~0.89 GPa, the lattice exhibits a stronger anisotropy in its compressibility: ~1% for a, ~0.4% for b, ~0.4% for c. This anisotropy suggests that at low P, the structure compresses preferentially along the a axis, indicating a tendency to reduce the voids between two-dimensional structural slabs that extend infinitely along the b and c axes [see Fig. 1(a)]. These slabs behave like rigid elements with similar compressibility along b and c, confirming the atomic connectivity scheme proposed for this compound (see Fig. 1). Above ~0.89 GPa, the anisotropy is effectively suppressed, marking a more isotropic lattice response to pressure. Note that all data included in Fig. 5(b) are experimental data based on diffraction datasets collected in this study. More details about these analyses are given in Supplemental Material [39].

III. DISCUSSION

Considering the $NbSe_3$ phase diagram, our electronical transport data show good agreement with the single-crystal x-ray diffraction results. The coexistence of $\boldsymbol{q_1}$ and $\boldsymbol{q_2}$ CDW wave vectors persists below ~0.8 GPa, consistent with a prior study [31]. Above ~2.9 GPa, the satellite reflections associated with both long-range CDW orders disappear, and superconductivity emerges. We emphasize that the disappearing of the CDW satellite reflections signifies the suppression of long-range CDW orders. Nevertheless, short-range or fluctuating CDW correlations might still persist beyond this pressure and could influence the transport properties. At this point, our results contrast to previous reports (e.g., Refs. [31,33,34]), which suggest a broad coexistence region between the long-range CDW and SC phases. In our study, the phase boundary is well defined and abrupt, as evidenced by the disappearance of the reflections associated with long-range $\boldsymbol{q_1}$ and $\boldsymbol{q_2}$ wave vectors and the suppression of the transport anomaly associated with the CDWs. These features occur specifically at ∼2.9 GPa, coinciding with the onset of SC. Such a sharply defined transition highlights a competitive interplay between the long-range CDW and SC phases and aligns with observations in other quasi-1D systems, such as $ZrTe_3$ [27] and Ta_2Se_8I [45], where SC emerges only after the long-range order is completely suppressed.

The primary structural distortion associated with both long-range CDWs in $NbSe_3$ involves selective displacements of Nb atoms: Nb(III) in the case of the $\boldsymbol{q_1}$-type modulation and Nb(I) for the $\boldsymbol{q_2}$-type modulation [6,36,38]. These distortions are accompanied by significant displacements of the surrounding Se atoms that coordinate Nb(III) and Nb(I), including those located on type II chains, whereas Nb(II) remains largely unaffected. These atomic displacements are attributed to the elastic intra- and interchain responses designed to minimize the Coulomb repulsion between individual CDWs.

At ambient pressure, the long-range CDW modulations on each pair of type III or type I chains are arranged out of phase, as reported in Refs. [36,37]. The type III chains (double chains) interact indirectly through intervening quadruple chains along the c direction. Within these quadruple chains, type I chains are wrapped by type II chains. Type II chains are believed to act as a polarizing medium for Coulomb interactions between the CDWs on the type I and type III chains [36]. These chains contribute to a closed Fermi surface (FS) via a less conductive, less 1D electronic band [7,46], in contrast to the open and flat FS, at ambient pressure, that originated from two highly conductive 1D d bands on the type III and type I chains which become gapped below T_{CDW1} and T_{CDW2}, respectively. Although the type II chains are not directly involved in the CDW formation, their electronic bands are influenced by CDW-induced charge redistribution. As pressure increases, the warping and hybridization [7,47] of the different FS sheets may become more pronounced, leading to degradation of the nesting. As seen in Fig. 1(e) for CDW1, the P-tuned α_1 sharply increases up to ∼0.8 GPa then decreases, which indicates the maximum reduction of density state at E_F for this P [48]. The α_1 decrease (with P) and increase (with impurity) phenomenon are both observed in previous works [31,48], with one report of constant α_1 [33]. This FS evolution in $NbSe_3$ contributes to the progressive suppression of the long-range CDW2 and CDW1 orders [31,46], which vanish at ∼0.8 GPa and ∼2.9 GPa, respectively.

The emergence of SC may relate to the closed FS pocket associated with the type II chain, the volume of which expands rapidly with P [38]. This FS pocket is not considered to be responsible for the CDW formation, but it relates to a Van Hove singularity in k space, where FSs of the differing dimensionality (1D band and 3D band) overlap. Such a scenario is again similar to the case of $ZrTe_3$ [27]. The increase of T_c in $NbSe_3$ with P, reaching a maximum of ∼4.5 K at ∼4.6 GPa, may be associated with the recovery of the density of state at the FS [46], as the system moves further away from the CDW-driven instability.

At pressure, below ∼0.8 GPa (LP) and temperatures of $T = 2$ and 10 K, n-type carriers dominate at low B values, but a crossover to p type occurs at higher B values. This field-induced carrier crossover suggests a strong connection between hole formation and the characteristics of the CDW2 state. For additional information, please see the discussion of Refs. [44,49], which propose that the emergence of p-type carriers at higher B may arise from quasiparticle excitations across a shrinking CDW gap on the hole surface. Additionally, the applied magnetic field B may further destabilize certain electronic states, enhancing hole contributions [50], as electrons condensed into the CDW ground state (charge transfer between normal carriers and the CDW condensate) [17]. For a given pressure above ambient and at higher temperatures, where the long-range CDW2 is fully suppressed, e.g., $T =$ 120 and 200 K, the system exhibits predominantly n-type conduction.

Above ∼0.8 GPa, the holelike CDW2 state is fully suppressed, and we find that n-type carriers become dominant across the entire range of applied magnetic fields and pressure. Notably, both the minima in R_H/d [Fig. 3(g)] and MR/B^2 [Fig. 3(h)] exhibit anomalies in the ∼0.8−1.3 GPa range, suggesting a correlation with the carrier-type crossover. Analysis of these transport signatures supports our observations, complete the overall picture, and indicate the coexistence, coupling, and competition of the long-range CDWs as a function of P and B.

We now turn to the discussion of the opposing shifts of q_1^{b*} and q_2^{b*} in the low-P CDW1 and CDW2 coexistence region. As shown in the inset of Fig. 5(a), the shifts preserve the relation $2(\boldsymbol{q_1} + \boldsymbol{q_2})$ ∼[111], which indicates the possibility of coupled CDW phases. The sharp increase of q_2^{b*} and decrease of q_1^{b*} is reminiscent of the shifts of q_1^{b*} and q_2^{b*} that are observed in samples carrying an electrical current in sliding CDWs [14–19,29], which was successfully reproduced by a model of charge transfer [16]. However, this extrapolated charge transfer model requires both CDWs to be depinned and decoupled, while there is no evidence in the present work that the two coexisting charge density waves (CDWs) are depinned below ∼0.8 GPa. In fact, although significant carrier redistribution occurs around ∼0.8 GPa, no corresponding increase in the resistivity anomaly associated with long-range CDW1 is observed. This suggests that phase coupling between the two CDWs remains robust under these conditions and is likely a key feature of their coexistence in $NbSe_3$. Still, the observed pressure dependence of the long-range CDW wave vectors raises further questions and calls for additional diffraction studies under uniaxial pressure to investigate how the joint commensurability of the CDWs evolves under both compressive and tensile strain applied along different crystallographic axes.

Suppression of CDWs under pressure is associated with a loss of long-range phase coherence, indicating that CDW ordering in $NbSe_3$ is closely tied to interchain phase relationships. These findings support the view that pressure not only modifies the lattice and electronic structure but also disrupts the collective CDW ground state through both structural and electronic pathways. Beyond 2.9 GPa, short-range or fluctuating CDW effect, without long-range order, may persist, as evidenced by rising T_C of SC, but it is not observed, neither as a CDW transport anomaly, nor as a diffraction reflection. The emergence of superconductivity in this regime highlights that long-range CDW order has been fully suppressed, while any residual short-range correlations do not prevent the formation of the superconducting state.

IV. CONCLUSIONS

Our results on x-ray diffraction, and transport properties measurements refine and extend our understanding of $NbSe_3$ and its phase diagram. The hypothesis of CDW and SC coexistence reported previously [31] (with phase labeled by $l+$SC and μ-SC) should be reconsidered. By analyzing the stability of CDW1 and CDW2, our data enable a detailed investigation of the dominant charge carrier types across a broad range of P, T, and B conditions. Importantly, we apply two complementary experimental techniques to $NbSe_3$ crystal sourced from the same synthesis batch, allowing for a more precise identification of sharp phase boundaries. X-ray diffraction data reveal subtle yet critical P-dependent changes in the satellite $\boldsymbol{q}$ vectors over a wide temperature range. These observations deepen our understanding of the long-range CDW-related phase transitions and provide insight into pressure-induced CDW periodicity changes.

From our observation, we propose the following scenario: (1) In the LP region (below ~0.8 GPa), the CDW1 and CDW2 coexist and joint commensurability is preserved [16]. (2) In the intermediate region (~0.8−1.3 GPa), the long-range CDW2 is suppressed and CDW1 is stabilized (anomaly of q_1^{b*}). (3) In the HP region (~1.3−2.9 GPa), the long-range CDW1 periodicity change becomes more pronounced. (4) Beyond ~2.9 GPa, SC emerges upon complete suppression of the long-range CDW1.

All these changes in the long-range CDWs appear to leave the main crystal lattice largely unaffected, as evidenced by the smooth evolution of lattice parameters. This suggests that the driving force originates primarily within the electronic system, or its coupling to lattice vibrations, manifesting in the atomic structure solely as distortions with their own periodicity. The observed interplay between structure, charge dynamics, and emergent phases calls for further studies to be performed using other probes such as inelastic x-ray scattering (IXS), but also to be performed using other stimuli, such as uniaxial pressure, where the strain cells here might be more favorable to carry out angle-resolved photoemission spectroscopy (ARPES).

ACKNOWLEDGMENTS

This work was supported by the Deutsches Elektronen-Synchrotron (DESY) Fellowship, by the Helmholtz-OCPC Postdoc Program of the China Postdoctoral Council (Grant No. 20191035), by the National Nature Science Foundation of China (Grants No. U1930401, No. 51527801, No. 12504177 and No. 51772184) and by the National Key R&D Program of China (Grant No. 2017YFA0403401). L.Y. was supported by the Fundamental Research Funds for Inner Mongolia University of Science & Technology under Grant No. 2024QNJS025. We acknowledge DESY (Hamburg, Germany) for the provision of their experimental facilities. Parts of the research were carried out at PETRA III at DESY, at beamlines P02.2 and P09, as well as at the DESY NanoLab [55]. We thank the beamline staff and the NanoLab team for their assistance. Beamtimes were allocated for proposals I-20200224, I-20200290, I-20221379, and I-20230421. We further acknowledge the "Bundesministerium fr Bildung und Forschung" under contract 05K13WC3 in the framework of the Verbundforschung "Characterization of exotic electronic und structural states of matter at extreme conditions IR- und THz-Spectroscopy at high and ultra-high pressures and variable temperature" (PI. N. Dubrovinskaia, Uni. Bayreuth) for the gas loading capacities at the ECSI and for the use of the FIB dual beam instrument to the DESY Nanolab.

DATA AVAILABILITY

The data that support the findings of this article are openly available [39].

[1] P. Monceau, Electronic crystals: An experimental overview, Adv. Phys. **61**, 325 (2012).

[2] T. Giamarchi, *Quantum Physics in One Dimension* (Clarendon Press, Oxford University Press, 2003), Vol. 121.

[3] J. L. Hodeau, M. Marezio, C. Roucau, R. Ayroles, A. Meerschaut, J. Rouxel, and P. Monceau, Charge-density waves in $NbSe_3$ at 145K: Crystal structures, X-ray and electron diffraction studies, J. Phys. C Solid State Phys. **11**, 4117 (1978).

[4] S. Nakamura and R. Aoki, Satellite electron-diffraction in $NbSe_3$ below $T = 59$ K, Solid State Commun. **27**, 151 (1978).

[5] J. A. Wilson, Bands, bonds, and charge-density waves in the $NbSe_3$ family of compounds, Phys. Rev. B **19**, 6456 (1979).

[6] S. van Smaalen, J. L. de Boer, A. Meetsma, H. Graafsma, H.-S. Sheu, A. Darovskikh, P. Coppens, and F. Levy, Determination of the structural distortions corresponding to the q^1 and q^2-type modulations in niobium triselenide $NbSe_3$, Phys. Rev. B **45**, 3103 (1992).

[7] J. Schäfer, E. Rotenberg, S. D. Kevan, P. Blaha, R. Claessen, and R. E. Thorne, High-temperature symmetry breaking in the electronic band structure of the quasi-one-dimensional solid $NbSe_3$, Phys. Rev. Lett. **87**, 196403 (2001).

[8] C. W. Nicholson, C. Berthod, M. Puppin, H. Berger, M. Wolf, M. Hoesch, and C. Monney, Dimensional crossover in a charge density wave material probed by angle-resolved photoemission spectroscopy, Phys. Rev. Lett. **118**, 206401 (2017).

[9] C. Brun, Z.-Z. Wang, and P. Monceau, Scanning tunneling microscopy at the $NbSe_3$ surface: Evidence for interaction between q_1 and q_2 charge density waves in the pinned regime, Phys. Rev. B **80**, 045423 (2009).

[10] E. C. Geil and R. E. Thorne, Spatially resolved transient dynamics of charge density waves in $NbSe_3$, Phys. Rev. Lett. **114**, 016404 (2015).

[11] C. Brun, Z.-Z. Wang, P. Monceau, and S. Brazovskii, Surface charge density wave phase transition in $NbSe_3$, Phys. Rev. Lett. **104**, 256403 (2010).

[12] M. A. Valbuena, P. Chudzinski, S. Pons, S. Conejeros, P. Alemany, E. Canadell, H. Berger, E. Frantzeskakis, J. Avila, M. C. Asensio, *et al.*, Polarization dependence of angle-resolved photoemission with submicron spatial resolution reveals emerging one-dimensionality of electrons in $NbSe_3$, Phys. Rev. B **99**, 075118 (2019).

[13] C. W. Nicholson, E. F. Schwier, K. Shimada, H. Berger, M. Hoesch, C. Berthod, and C. Monney, Role of a higher-dimensional interaction in stabilizing charge density waves in quasi-one-dimensional $NbSe_3$ revealed by angle-resolved photoemission spectroscopy, Phys. Rev. B **101**, 045412 (2020).

[14] R. M. Fleming, D. E. Moncton, and D. B. McWhan, X-ray scattering and electric field studies of the sliding mode conductor $NbSe_3$, Phys. Rev. B **18**, 5560 (1978).

[15] S. Brazovskii, N. Kirova, H. Requardt, F. Y. Nad, P. Monceau, R. Currat, J. E. Lorenzo, G. Grübel, and C. Vettier, Plastic sliding of charge density waves: X-ray space resolved-studies versus theory of current conversion, Phys. Rev. B **61**, 10640 (2000).

[16] A. Ayari, R. Danneau, H. Requardt, L. Ortega, J. E. Lorenzo, P. Monceau, R. Currat, S. Brazovskii, and G. Grübel, Sliding-induced decoupling and charge transfer between the coexisting q_1 and q_2 charge density waves in $NbSe_3$, Phys. Rev. Lett. **93**, 106404 (2004).

[17] A. A. Sinchenko, R. V. Chernikov, A. A. Ivanov, P. Monceau, T. Crozes, and S. A. Brazovskii, Hall effect in the pinned and sliding charge density wave state of $NbSe_3$, J. Phys. Condens. Matter **21**, 435601 (2009).

[18] A. A. Sinchenko, P. Monceau, and T. Crozes, Transverse conductivity in the sliding charge-density-wave state of $NbSe_3$, Phys. Rev. Lett. **108**, 046402 (2012).

[19] A. V. Frolov, A. P. Orlov, A. A. Sinchenko, and P. Monceau, Charge density wave sliding driven by an interplay of conventional and Hall voltages in $NbSe_3$ microbridges, Phys. Rev. B **100**, 245126 (2019).

[20] C. Lin, M. Ochi, R. Noguchi, K. Kuroda, M. Sakoda, A. Nomura, M. Tsubota, P. Zhang, C. Bareille, K. Kurokawa, *et al.*, Visualization of the strain-induced topological phase transition in a quasi-one-dimensional superconductor $TaSe_3$, Nat. Mater. **20**, 1093 (2021).

[21] S. Ricco, M. Kim, A. Tamai, S. McKeown Walker, F. Y. Bruno, I. Cucchi, E. Cappelli, C. Besnard, T. K. Kim, P. Dudin, *et al.*, *In situ* strain tuning of the metal-insulator-transition of Ca_2RuO_4 in angle-resolved photoemission experiments, Nat. Commun. **9**, 4535 (2018).

[22] A. F. Isakovic, P. G. Evans, J. Kmetko, K. Cicak, Z. Cai, B. Lai, and R. E. Thorne, Shear modulus and plasticity of a driven charge density wave, Phys. Rev. Lett. **96**, 046401 (2006).

[23] B. Yue, W. Zhong, H. Zhang, J. Zhou, J. Miao, S. Kawaguchi, H. Kadobayashi, and F. Hong, Pressure-induced superconductivity in quasi-one-dimensional ZrS_3, Phys. Rev. B **110**, 144515 (2024).

[24] Z. Y. Liu, Q. X. Dong, P. T. Yang, P. F. Shan, B. S. Wang, J. P. Sun, Z. L. Dun, Y. Uwatoko, G. F. Chen, X. L. Dong, Z. X. Zhao, and J.-G. Cheng, Pressure-induced superconductivity up to 9 K in the quasi-one-dimensional KMn_6Bi_5, Phys. Rev. Lett. **128**, 187001 (2022).

[25] S. Yasuzuka, Y. Okajima, S. Tanda, N. Takeshita, N. Môri, and K. Yamaya, Pressure-induced magnetoresistance in $NbSe_3$, J. Phys. Soc. Jpn. **69**, 3470 (2000).

[26] M. Hoesch, G. Garbarino, C. Battaglia, P. Aebi, and H. Berger, Evolution of the charge density wave superstructure in $ZrTe_3$ under pressure, Phys. Rev. B **93**, 125102 (2016).

[27] R. Yomo, K. Yamaya, M. Abliz, M. Hedo, and Y. Uwatoko, Pressure effect on competition between charge density wave and superconductivity in $ZrTe_3$: Appearance of pressure-induced reentrant superconductivity, Phys. Rev. B **71**, 132508 (2005).

[28] S. L. Gleason, Y. Gim, T. Byrum, A. Kogar, P. Abbamonte, E. Fradkin, G. J. MacDougall, D. J. Van Harlingen, X. Zhu, C. Petrovic, and S. L. Cooper, Structural contributions to the pressure-tuned charge-density-wave to superconductor transition in $ZrTe_3$: Raman scattering studies, Phys. Rev. B **91**, 155124 (2015).

[29] D. DiCarlo, E. Sweetland, M. Sutton, J. D. Brock, and R. E. Thorne, Field-induced charge-density-wave deformations and phase slip in $NbSe_3$, Phys. Rev. Lett. **70**, 845 (1993).

[30] R. Bruinsma and S. E. Trullinger, Phase-locked charge-density waves in $NbSe_3$, Phys. Rev. B **22**, 4543 (1980).

[31] S. Yasuzuka, K. Murata, T. Fujimoto, M. Shimotori, and K. Yamaya, Coexistence of the upper charge-density-wave and the superconductivity in $NbSe_3$, J. Phys. Soc. Jpn. **74**, 1782 (2005).

[32] S. Yasuzuka, K. Yamaya, Y. Okajima, S. Tanda, N. Takeshita, H. Mitamura, T. Nakanishi, and N. Môri, Violation of Kohler's rule in the magnetoresistance near the lower charge-density-wave instability in $NbSe_3$, J. Phys. Soc. Jpn. **74**, 1787 (2005).

[33] M. Ido, Y. Okayama, T. Ijiri, and Y. Okajima, Pressure effect on the charge-density waves and the superconductivity in $NbSe_3$, J. Phys. Soc. Jpn. **59**, 1341 (1990).

[34] M. N. Regueiro, J. M. Mignot, and D. Castello, Superconductivity at high pressure in $NbSe_3$, Europhys. Lett. **18**, 53 (1992).

[35] S. Yasuzuka, Y. Okajima, S. Tanda, K. Yamaya, N. Takeshita, and N. Môri, Pressure effect on large magnetoresistance in the lower charge-density-wave transition of $NbSe_3$, Phys. Rev. B **60**, 4406 (1999).

[36] E. Canadell, I. E. I. Rachidi, J. P. Pouget, P. Gressier, A. Meerschaut, J. Rouxel, D. Jung, M. Evain, and M. H. Whangbo, Comparison of the electronic structures of layered transition-metal trichalcogenides thallium triselenide, thallium trisulfide and niobium triselenide, Inorg. Chem. **29**, 1401 (1990).

[37] B. Guster, M. Pruneda, P. Ordejón, E. Canadell, and J.-P. Pouget, Basic aspects of the charge density wave instability of transition metal trichalcogenides $NbSe_3$ and monoclinic-TaS_3, J. Phys. Condens. Matter **33**, 485401 (2021).

[38] J. A. Wilson, Concerning the discommensurate character of $NbSe_3$, J. Phys. F Met. Phys. **12**, 2469 (1982).

[39] See Supplemental Material at http://link.aps.org/supplemental/10.1103/s48z-19pt for experimental details and additional single-crystal x-ray diffraction results on $NbSe_3$, which also includes Refs. [51–56].

[40] R. V. Coleman, M. P. Everson, H.-A. Lu, A. Johnson, and L. M. Falicov, Effects of high magnetic fields on charge-density waves in $NbSe_3$, Phys. Rev. B **41**, 460 (1990).

[41] N. P. Ong and P. Monceau, Anomalous transport properties of a linear-chain metal: $NbSe_3$, Phys. Rev. B **16**, 3443 (1977).

[42] J. Hyun, Y. Lee, C.-y. Lim, G. Lee, J. Cha, Y. Ahn, M. Jho, S. Gim, M. Park, M. Hashimoto, D. Lu, Y. Kim, and S. Kim, Band-selective spin-charge separation across the charge

density wave transition in quasi-1D $NbSe_3$, Phys. Rev. Lett. **134**, 206402 (2025).

[43] M. P. Everson, G. Eiserman, A. Johnson, and R. V. Coleman, Electric field dependence of the Hall effect in $NbSe_3$, Phys. Rev. B **30**, 3582 (1984).

[44] N. P. Ong and P. Monceau, Hall effect of a linear-chain metal: $NbSe_3$, Solid State Commun. **26**, 487 (1978).

[45] Q.-G. Mu, D. Nenno, Y. -P. Qi, F.-R. Fan, C. Pei, M. ElGhazali, J. Gooth, C. Felser, P. Narang, S. Medvedev, *et al.*, Suppression of axionic charge density wave and onset of superconductivity in the chiral Weyl semimetal Ta_2Se_8I, Phys. Rev. Mater. **5**, 084201 (2021).

[46] S. Wada, M. Kaburagi, Y. Saito, and R. Aoki, Superconductivity enhancement and CDW gap formation-NMR study of the pressure and impurity effects in $NbSe_3$, J. Phys. F Met. Phys. **18**, 1231 (1988).

[47] J. Schäfer, M. Sing, R. Claessen, E. Rotenberg, X. J. Zhou, R. E. Thorne, and S. D. Kevan, Unusual spectral behavior of charge-density waves with imperfect nesting in a quasi-one-dimensional metal, Phys. Rev. Lett. **91**, 066401 (2003).

[48] K. Kawabata, Impurity effects on superconductivity and charge density waves in $NbSe_3$, J. Phys. Soc. Jpn. **54**, 762 (1985).

[49] N. P. Ong, Two-band model for $NbSe_3$ (Ohmic regime), Phys. Rev. B **18**, 5272 (1978).

[50] M. F. Hundley and A. Zettl, Magnetothermopower of $NbSe_3$, Solid State Commun. **61**, 587 (1987).

[51] A. G. Gavriliuk, A. A. Mironovich, and V. V. Struzhkin, Miniature diamond anvil cell for broad range of high pressure measurements, Rev. Sci. Instrum. **80**, 043906 (2009).

[52] H. Mao, J.-A. Xu, and P. Bell, Calibration of the ruby pressure gauge to 800 kbar under quasi-hydrostatic conditions, J. Geophys. Res. **91**, 4673 (1986).

[53] A. Celeste, F. Borondics, and F. Capitani, Hydrostaticity of pressure-transmitting media for high pressure infrared spectroscopy, High Pressure Res. **39**, 608 (2019).

[54] Rigaku Oxford Diffraction, CrysAlis Pro software system, version 1.171.41.122a, Rigaku Corporation, Wroclaw, Poland (2022).

[55] A. Stierle, T. F. Keller, H. Noei, V. Vonk, and R. Roehlsberger, Desy NanoLab, JLSRF **2**, A76 (2016).

[56] S. Kikkawa, N. Ogawa, M. Koizumi, and Y. Onuki, High-pressure syntheses of TaS_3, NbS_3, $TaSe_3$, and $NbSe_3$ with $NbSe_3$-type crystal structure, J. Solid State Chem. **41**, 315 (1982).